

# AQuaRef: Machine learning accelerated quantum refinement of protein structures

Roman Zubatyuk<sup>1,#</sup>, Malgorzata Biczysko<sup>2,#</sup>, Kavindri Ranasinghe<sup>3,#</sup>, Nigel W. Moriarty<sup>4</sup>  
Hatice Gokcan<sup>1</sup>, Holger Kruse<sup>6</sup>, Billy K. Poon<sup>4</sup>, Paul D. Adams<sup>4,5</sup>, Mark P. Waller<sup>6</sup>,  
Adrian E. Roitberg<sup>3</sup>, Olexandr Isayev<sup>1,\*</sup>, Pavel V. Afonine<sup>4,\*</sup>

<sup>1</sup> *Department of Chemistry, Carnegie Mellon University, Pittsburgh, PA 15213, USA*

<sup>2</sup> *Faculty of Chemistry, University of Wrocław, F. Joliot-Curie 14, 50-383 Wrocław, Poland*

<sup>3</sup> *Department of Chemistry, University of Florida, Gainesville, FL 32611, USA*

<sup>4</sup> *Molecular Biophysics & Integrated Bioimaging Division, Lawrence Berkeley National Laboratory, Berkeley, CA 94720-8235, USA*

<sup>5</sup> *Department of Bioengineering, University of California Berkeley, Berkeley, CA 94720, USA*

<sup>6</sup> *Pending.AI, Eveleigh, NSW 2015, Australia*

# These authors contributed equally

\*Corresponding authors: P.V.A. - [PAfonine@LBL.Gov](mailto:PAfonine@LBL.Gov),

O.I. - [olexandr@olexandrisayev.com](mailto:olexandr@olexandrisayev.com)

## ABSTRACT

Cryo-EM and X-ray crystallography provide crucial experimental data for obtaining atomic-detail models of biomacromolecules. Refining these models relies on library-based stereochemical restraints, which, in addition to being limited to known chemical entities, do not include meaningful noncovalent interactions relying solely on nonbonded repulsions. Quantum mechanical (QM) calculations could alleviate these issues but are too expensive for large molecules. We present a novel AI-enabled Quantum Refinement (AQuaRef) based on AIMNet2 neural network potential mimicking QM at substantially lower computational costs. By refining 41 cryo-EM and 30 X-ray structures, we show that this approach yields atomic models with superior geometric quality compared to standard techniques, while maintaining an equal or better fit to experimental data.

## INTRODUCTION

While advances in predictive modeling, such as AlphaFold3<sup>1</sup> or RoseTTAFold<sup>2,3</sup>, have provided powerful tools for structural biology, they remain limited while experimental methods, including protein crystallography and cryo-EM, are still cornerstones of structural biology and drug development<sup>4</sup>. Experimental data allow for the discovery of new structures emerging in life evolution, potentially exhibiting previously unseen features. These discoveries require unbiased information provided by experiments to explore the unknown<sup>5</sup>. Atomic model refinement is a crucial near-final stage in crystallographic or cryo-EM structure determination aimed at producing molecular models that meet standard validation criteria while optimally fitting the experimental data<sup>6</sup>. Refinement heavily relies on stereochemical restraints to maintain the correct geometry of the atomic model while fitting to the experimental data<sup>7</sup>. These restraints originate from standard libraries that tabulate the topology and parameters of known chemical entities<sup>8,9</sup>, which are universally employed across popular software packages, such as CCP4<sup>10</sup> and Phenix<sup>11</sup>.

The limitations of library-based restraints are manifold. Firstly, they only include terms for maintaining covalent bond lengths, bond angles, torsion angles, planes and chirality while preventing clashes through non-bonded repulsion<sup>12</sup>. However, it has been demonstrated

that at low resolution, these restraints are insufficient to maintain realistic, chemically meaningful macromolecular geometries, making it essential to include additional restraints on protein main chain  $\phi/\psi$  angles, side chain torsion  $\chi$  angles, as well as hydrogen bond parameters and  $\pi$ -stacking interactions to stabilize protein or nucleic acid secondary structure<sup>12–18</sup>. These additional restraints cannot be reliably inferred from the atomic model alone and thus require manual error-prone annotation and curation using additional sources of information, such as homologous high-resolution models. Secondly, library-based restraints parametrize only known chemical entities, such as standard amino and nucleic acids as well as previously defined ligands. Consequently, any nonstandard entities or interactions, such as novel ligands or covalent cross-chain links, require manual annotation and definition, without which refinement may fail to proceed correctly or at all. Finally, deviations from standard covalent geometry due to local chemical interactions are not uncommon<sup>19–21</sup>. While these deviations are valid, restraints may interpret them as violations requiring 'correction'.

The advantage of using simple restraints<sup>7</sup> is the minimal computational cost they add to the refinement workflow. A possible next step is to use a classical force field to account for geometric elements<sup>22</sup>. However, these force fields have their own set of limitations: they require parametrization for new chemical species and cannot distinguish between chemically equivalent bonds in different chemical environments.

Quantum refinement is a fundamentally different approach, balancing the fitting to experimental data with a term related to the quantum mechanical energy of the system<sup>23,24</sup>. It has been demonstrated that the entire atomic model can benefit from a full QM treatment<sup>25–27</sup>. Figure 1 presents a timeline showcasing the evolution of quantum mechanics calculations for proteins, highlighting four key stages of progress and advancements in technology and methodology. Traditionally, quantum refinements were deemed impractical for macromolecules due to the computational requirements. Methods often focused solely on the macromolecular region of interest, such as a ligand-binding pocket or enzyme active site, while employing a classical approach for the rest of the molecule<sup>28,29</sup>. Numerous approaches and implementations have been reported over time<sup>30</sup>, with GPU-accelerated codes enabling QM calculations for peptides and small

proteins of a few hundred atoms being one of the most prominent milestones<sup>31</sup>. Interaction-based model partitioning into chemically meaningful fragments<sup>32</sup> solved the scalability issue in quantum calculations<sup>26</sup>, which in turn enabled the refinement of larger proteins. However, this approach remained computationally demanding.



**Figure 1.** Timeline illustrating the progression of quantum mechanics calculations applied to proteins, emphasizing four critical stages marked by advancements in technology and methodology.

Refinement of selected cryo-EM and X-ray atomic models across various resolutions demonstrates the AQuaRef's ability to produce atomic models with superior geometric quality compared to conventional techniques while maintaining or improving agreement with experimental data. This work represents the first example where machine learning (ML) potentials have been adopted to perform quantum refinement of the entire protein, in contrast with a recent approach where ML potentials have been combined with the ONIOM-like QM/MM partitioning<sup>38</sup>.

## RESULTS

Conceptually, quantum-based atomic model refinement is very similar to classic refinement wherein atomic model parameters are iteratively adjusted in order to minimize the residual,  $T = T_{data} + w * T_{restraints}$ . Here,  $T_{data}$  describes the fit of the model to the data and  $T_{restraints}$  incorporates chemical restraints with an *a-priori* unknown weight,  $w$ <sup>[39]</sup>.

However, there are four fundamental differences. First, in QM refinement, restraints are derived from quantum-mechanical calculations for the specific macromolecule in consideration. Second, the requirements for the initial atomic model in QM refinement are stricter compared to standard refinement: the atomic model must be correctly protonated, atom-complete and free of severe geometric violations such as steric clashes or broken covalent bonds<sup>23,24</sup>. Third, while crystallographic software packages inherently account for crystal symmetry, QM codes generally do not. Fourth, crystallographic software is capable of handling static disorder that is modeled with alternative conformations, whereas QM codes typically lack this capability. All these nuances specific to quantum refinement (except handling static disorder, which is a current limitation) are addressed in the Quantum Refinement package (Q|R)<sup>23,26,27,40</sup>, which is being developed as part of this work and provides the necessary procedures to enable quantum refinement within the Phenix software.

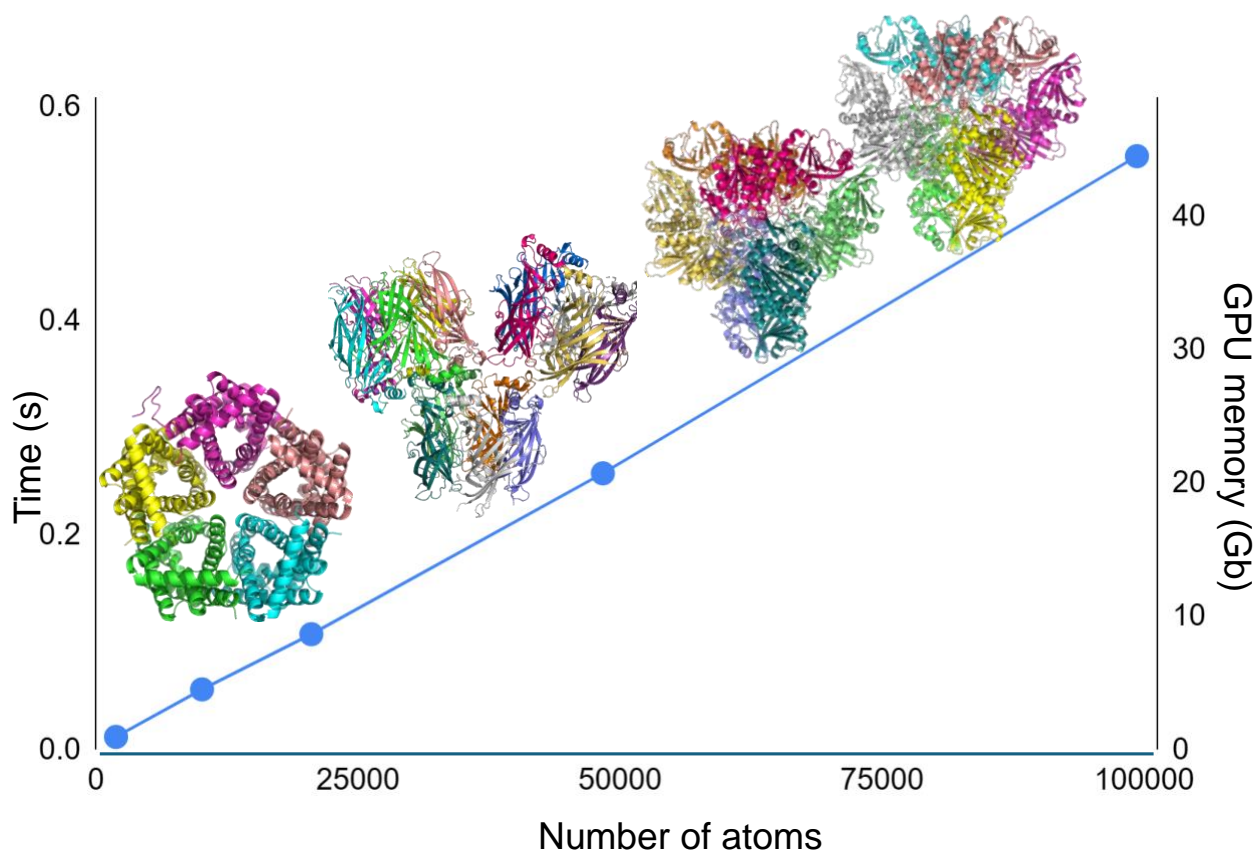


**Figure 2.** Computational scaling of the AIMNet2 neural network model in AQuaRef. Time to compute energy and forces (left axis) and peak GPU memory usage (right axis) versus the number of atoms in the system. Calculations are performed on a single Nvidia H100 PCIe 80GB GPU.

Conventional QM methods like density functional theory (DFT) for  $N$ -electron systems require  $O(N^2)$  storage and  $O(N^3)$  arithmetic operations. This  $O(N^3)$  complexity is a critical bottleneck that limits the ability to study large realistic biological systems like proteins. Figure 2 shows the computational scaling of the AIMNet2 model, where both energy and force calculations, as well as peak GPU memory usage, scale linearly ( $O(N)$ ) with system size. For a large protein system of 100,000 atoms, single-point energy and forces can be computed in 0.5 seconds. Overall, an atomic model consisting of approximately 180,000 atoms can fit into the 80GB memory of a single NVIDIA H100 GPU.

We tested the new quantum refinement procedure on 41 cryo-EM atomic models, 20 low-resolution and 10 very high-resolution X-ray atomic models. Standard stereochemistry<sup>41,42</sup> and model-to-data fit criteria<sup>43–45</sup>, MolProbity validation tools<sup>46</sup> along with newly developed metrics to evaluate hydrogen bond quality<sup>18</sup> were used to assess the atomic models. Typically, the time needed for quantum refinement is about twice as long as standard refinement, and often shorter than the standard refinement with additional restraints such as the Ramachandran plot, secondary structure and side-chain rotamer restraints<sup>47–50</sup>. Quantum refinement takes under 20 minutes in about 70% of models considered in this work, with a maximum of about 1 hour (Supplementary Data: Table 6). These computations can be performed on GPU-equipped laptops, with the only limitation being available GPU memory.

## Quantum refinement

The AQuaRef refinement procedure begins with a check for the completeness of the atomic model, followed by the addition of any missing atoms. This may result in steric clashes, particularly if the model was previously refined without hydrogen atoms. Models with missing atoms that cannot be trivially added (e.g., missing main chain atoms) cannot be used for quantum refinement. If clashes or other severe geometric violations are detected, quick geometry regularization is performed using standard restraints, ensuring that atoms move as little as necessary to resolve the clashes. For crystallographic refinement, to account for interactions arising from crystallographic symmetry and periodicity of unit cells, the model is expanded into a supercell by applying appropriate space group symmetry operators<sup>25</sup>. Subsequently, it is truncated to retain only parts of the symmetry copies within a prescribed distance from atoms of the main copy<sup>40</sup>. This step is unnecessary for refinement against cryo-EM data. The atom-completed and expanded model then undergoes the standard atomic model refinement protocol as implemented in Q|R package<sup>23</sup>.

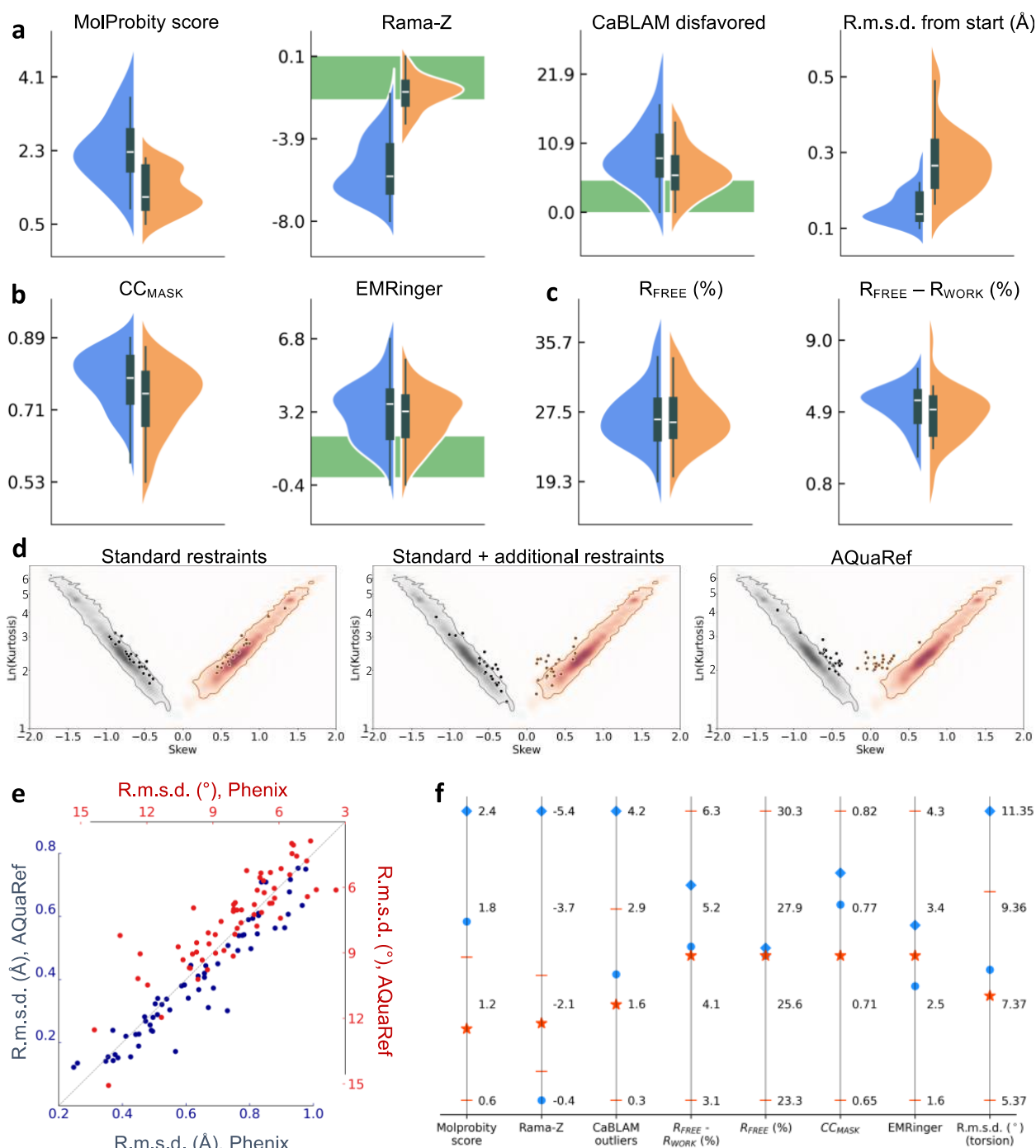


**Figure 3. a-d:** Summary of refinements of 41 low-resolution cryo-EM models and 20 low-resolution X-ray models using standard stereochemistry (blue) and AQuaRef (orange) restraints (Supplementary Data: Table 1). **a:** MolProbity score, Ramachandran plot Z-

score, CaBLAM disfavored and r.m.s. deviation of refined model from initial model. **b**: cross-correlation between experimental and model-generated maps ( $CC_{\text{mask}}$ ), and EMRinger score for cryo-EM models. **c**:  $R_{\text{free}}$  and  $R_{\text{free}}-R_{\text{work}}$  for X-ray models (Supplementary Data: Table 3). Green band indicates favored range of corresponding values. **d**: skew-kurtosis plots for hydrogen bond parameters (Hydrogen(H)...Acceptor(A) distances and Donor-H...A angles) for refinements using (left-to-right): standard restraints; standard restraints with addition of Ramachandran plot, secondary-structure and side-chain rotamer restraints; and AQuaRef restraints. **e**: r.m.s. deviations between refined and high-resolution homology models, refinements using standard versus AQuaRef restraints, calculated using matching Cartesian coordinates (blue, lower-left) and matching torsion angles (red, upper-right) (Supplementary Data: Tables 2,4). **f**: summary of mean values, for all test refined models: MolProbity score, Ramachandran Z-score, CaBLAM outliers, r.m.s. deviation of matching torsion angles between refined and high-resolution homologous models, as well as  $R_{\text{free}}-R_{\text{work}}$  and  $R_{\text{free}}$  for X-ray models and  $CC_{\text{mask}}$  and EMRinger score for cryo-EM models for refined models with standard restraints (blue rhombi), standard restraints with addition of Ramachandran plot, secondary-structure and side-chain rotamer restraints (blue circles); and AQuaRef restraints (red stars). Red bars show standard deviations for starred values.

### **Application of the new refinement procedure to a set of deposited atomic models**

To evaluate the performance of the new QM-based refinement, we refined 41 low-resolution cryo-EM atomic models, 20 low-resolution and 10 ultra-high-resolution X-ray atomic models, which contain only proteins. All selected 61 low-resolution atomic models have high-resolution homologs, which were used as the ground truth for comparison (Supplementary Data: Tables 2,4). Refinements were carried out using three sets of restraints: QM restraints from AIMNet2 (AQuaRef refinement); standard restraints; and standard restraints plus additional restraints on hydrogen bonds and angles involved in maintaining secondary structure, main-chain  $\phi/\psi$  angles (Ramachandran plot restraints) and side-chain torsion  $\chi$  angles (rotamer restraints).

Overall, low-resolution atomic models after quantum refinement exhibit systematically superior geometry quality compared to those obtained using standard restraints, as indicated by their MolProbity scores<sup>51</sup>, Ramachandran Z-scores<sup>52</sup>, CaBLAM disfavored<sup>46</sup> (Fig. 3a), and skew-kurtosis plots for hydrogen bond parameters<sup>18</sup> (Fig. 3d). They also systematically deviate more from the initial coordinates. These atomic models demonstrate a very similar fit to the experimental data (Fig. 3b,c), with slightly less data overfitting for X-ray atomic models, as evidenced by a smaller  $R_{\text{work}}-R_{\text{free}}$  gap and similar  $R_{\text{free}}$ <sup>[53,54]</sup>. Since there is no equally efficient control over overfitting in cryo-EM as there is with  $R_{\text{free}}$  in crystallography, the slightly lower cross-correlation between experimental and model-calculated masked maps ( $CC_{\text{mask}}$ )<sup>43</sup> and essentially the same EMRinger scores<sup>55</sup>, together with significantly improved atomic model geometry, likely indicate a reduction in overfitting. Augmenting standard restraints with secondary structure, Ramachandran plot and side-chain rotamer restraints expectedly improves the geometry (Fig. 3d,f), yet using AQuaRef still produces superior atomic model geometries. With a few exceptions, atomic models refined with quantum restraints are systematically closer to their higher-resolution homologs compared to those using standard restraints alone or complemented with additional restraints (Fig. 3e,f). In some of the most remarkable cases, the local structure obtained with AQuaRef restraints closely matches the high-resolution homologs and differs from those obtained using standard restraints by up to two Angstroms (Fig. 4 a-c).

## DISCUSSION

Here, we present AQuaRef, a novel approach to the quantum refinement of entire protein structures, made possible by using ML-accelerated quantum mechanical calculations with AIMNet2. For the first time, this allows for the refinement of full atomic models of realistic protein structures using stereochemical restraints derived from quantum mechanical calculations.

Test refinements using 61 low-resolution X-ray and cryo-EM atomic models show systematic improvements in geometric validation criteria by using QM restraints while maintaining a similar fit to the experimental data and reducing overfitting. The presence of high-resolution homologous atomic models, which are expected to better represent the

actual true structures than low-resolution atomic models, allowed us to assess whether these improvements are associated with refined structures becoming closer to the true ones. With a few exceptions, we find that atomic models refined with AQuaRef restraints are systematically closer to their high-resolution matches. This indicates that QM-based refined atomic models not only improve standard validation metrics but also provide more realistic representations of the true structures compared to atomic models refined with standard restraints. Expectedly, refining 10 very high-resolution atomic models did not significantly alter the atomic coordinates but did lead to improved *R*-factors for all ten models (Supplementary Data: Table 5). The most notable differences compared to refinement with standard restraints were observed in the position of hydrogen atoms, specifically those with rotational degrees of freedom (Fig. 4 d-g), where some of these atoms reoriented during refinement to better fit the data and, at the same time, form favorable hydrogen bonds. Another notable difference is the increased r.m.s. deviations from ideal (library) bond and angle values in the case of AQuaRef refinement (Supplementary Data: Table 5), which together with improved hydrogen positions is likely to contribute to improved *R*-factors.

The method has been implemented in the quantum refinement software (Q|R), which is built upon the CCTBX library<sup>56</sup> and optionally utilizes tools from Phenix. Q|R is accessible within Phenix, thereby making these methods readily available to the broader community of structural biologists.

Currently, AQuaRef is trained using commonly known amino acid residues, which means the method can only be applied to protein-only structures. Another main limitation is that, at present, static disorder (alternate conformations) is not handled in Q|R. Removing both limitations is the subject of future work.

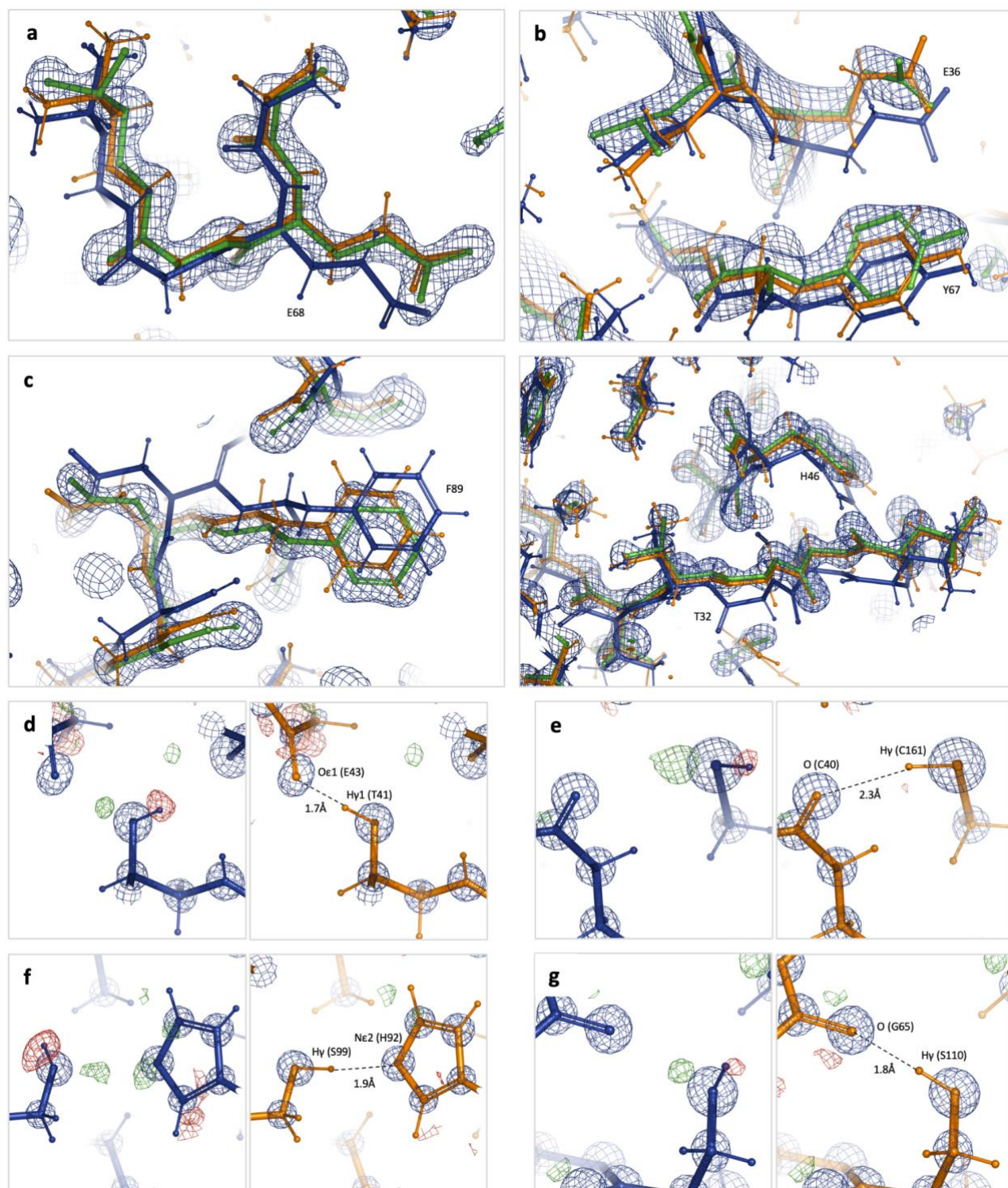


**Figure 4. a-c:** Close-up showing models refined with standard restraints (blue) and AQUaRef restraints (orange) superposed onto their higher-resolution homologous models (green) with their corresponding 2mFo-DFc Fourier maps contoured at 2σ; for PDB 5YI5, 8R1G, and 6XMV, respectively. **d-g:** Refinement with standard AQUaRef restraints

(orange) overlaid with their corresponding 2mFo-DFc and mFo-DFc Fourier maps, contoured at  $5\sigma$  (blue) and  $\pm 2\sigma$  (green, red), respectively (PDB 4O8H). The focus is on hydrogen atoms with rotational degrees of freedom that re-orient during refinement with AQuaRef restraints to satisfy the residual map and participate in hydrogen bonding.

## METHODS

### **AIMNet2 training dataset and AQuaRef model**

Since our goal was the parametrization of ML potential for polypeptides, our training dataset needed to cover chemical (amino acid sequence and protonation states), conformational, and intermolecular degrees of freedom. We began by creating a library of small peptides as SMILES strings. We used all 20 standard amino acids, 11 alternate protonation forms, three options for sequence start (ACE, NH<sub>3</sub><sup>+</sup>, NH<sub>2</sub>), and four options for the end (NME, NHE, CBX, CBA). We enumerated all possible mono- and di-peptides and selected a random subset for tri- and tetra-peptides. Additionally, we generated SMILES for peptides linked by the cysteine-cysteine disulfide bond and their selenium counterparts. Molecular conformations were generated with OpenEye Omega<sup>57</sup> software using dense torsion sampling. No restrictions were applied to the configurations of the chiral centers, ensuring that the dataset and resulting model should work equally well for D-, L-, and mixed stereochemistry peptides. Intermolecular interactions were modeled by generating intermolecular complexes of 2 to 4 peptides with random orientations. No prior knowledge of preferred types of secondary structure for polypeptides was used. To manage the size of the dataset and the training process, we limited the size of peptides and complexes to less than 120 atoms, including hydrogens.

Non-equilibrium conformations of peptides and complexes were sampled with molecular dynamics simulations using the GFN-FF<sup>58</sup> force field. Cartesian restraints were added to keep structures near the input structure, with random torsion and intermolecular degrees of freedom. Molecular configurations for labeling (DFT calculations) and inclusion into the training dataset were selected using Query-By-Committee active learning (AL) approach<sup>35</sup>. We started with a random selection of 500k samples, used an ensemble of

4 models, and performed a total of 4 iterations of AL adding new samples with high uncertainty of energy and atomic forces prediction. In the final iteration of AL, we performed uncertainty-guided optimization of the structures, minimizing the weighted difference of energy prediction and its uncertainty. This type of active sampling finds structures that balance low predicted forces and high energy uncertainty. The entire procedure resulted in a training dataset containing about one million samples, with a median number of 42 atoms per sample.

DFT calculations were performed with the B97M-D4/def2-QZVP<sup>59–62</sup> method using ORCA 5.0.3 software<sup>63</sup>. Since the Q|R does not use periodic boundary conditions, and usually not all ions and solvent molecules are resolved in the refinement, we used implicit treatment of solvent effects with CPCM<sup>64</sup> method using parameters for water as solvent.

The core architecture of the AQuaRef model matches the base AIMNet2 model<sup>33</sup>, with few modifications. First, we did not use explicit long-range Coulomb and dispersion interactions, we trained to total DFT-D4 energy instead. With CPCM treatment, the Coulomb term could not be estimated using interactions between partial atomic charges, and also long-range interactions are effectively screened with a polarizable continuum. Long range dispersion interactions beyond the local cutoff of 5 Å have little effect on atomic forces, which are important in Q|R refinement. We also added explicit short-range exponential repulsion terms to make the potential more robust for the structures with clashes. The model was trained to reproduce DFT-D4 energies, forces, and Hirshfeld partial atomic charges.

## **Experimental data and atomic models for test cases**

Protein-only, single-conformation high-to-low resolution X-ray crystallography and Cryo-EM models, along with their corresponding experimental datasets, were selected from RCSB and EMDB based on multiple criteria. These criteria include model size (between 1,000 and 10,000 non-hydrogen atoms), resolution (between 2.5 and 4 Å), geometric model quality (MolProbity clashscore better than 50, with no covalent bonds deviating by more than 4 r.m.s.d. from ideal library values), goodness of fit between the model and the

experimental data (Cryo-EM:  $CC_{\text{mask}} > 0.6$ , X-ray:  $R_{\text{work}} < 0.3$ ), and the availability of a higher-resolution (better than 2 Å) homologous model (main chain superposition r.m.s.d.  $< 1$  Å, sequence identity greater than 95%) for each considered model. Additionally, 11 ultra-high resolution single-conformation X-ray models were selected that contained only protein and ordered water atoms.

## Comparison of models

All atoms were used to calculate coordinate r.m.s. deviations between models before and after refinement, as shown in Figure 3a. Coordinate r.m.s. deviations between models used for test refinements and their high-resolution homologues were calculated using the Phenix tool `phenix.superpose_pdbs`, which included all non-hydrogen backbone atoms plus C $\beta$  and C $\gamma$  atoms where present. R.m.s. deviations in torsion angle space were calculated using CCTBX<sup>56</sup>, with matching torsion angles selected as described by Headd et al.<sup>15</sup>.

## Atomic model preparation for refinement

Model preparation for refinement (e.g., adding any missing atoms) was done using `qr.finalise` program of Q|R, which uses the Reduce program<sup>65</sup> to add hydrogen atoms at geometrically predicted positions. Model geometry regularization was done using the Phenix tool `phenix.geometry_minimization`.

## Model refinement

The exact same input models were used for all trial refinements. Real-space refinement in Phenix was performed using the `phenix.real_space_refine` program<sup>12</sup>. Four refinement runs were performed independently, starting with the same input maps (cryo-EM) or reflection data (X-ray) and models. The runs included: 1) standard restraints consisting of restraints on bond lengths, bond angles, torsion angles, planes, chirality, and non-

bonded repulsion; 2) standard restraints with the addition of secondary-structure restraints; 3) standard restraints with the addition of Ramachandran plot restraints; and 4) standard restraints with the addition of secondary-structure and Ramachandran plot restraints.

Quantum-based real- and reciprocal-space refinement was performed using the qr.refine program of Q|R, using all default settings except for the source of QM restraints (AQuaRef).

Reciprocal-space refinement in Phenix was performed using phenix.refine<sup>66</sup> with the exact same four choices of restraints as in real-space refinement.

## Software and availability

Phenix software is available at: [phenix-online.org](http://phenix-online.org). Quantum refinement (Q|R) software is available at [qrefine.com](http://qrefine.com). AQuaRef refinement is available in Phenix starting dev-5395 version. CCTBX-based Python scripts and the data (atomic models, cryo-EM maps, X-ray diffraction data) used in this study are available at: [https://phenix-online.org/phenix\\_data/afonine/qr\\_aimnet2\\_2024/](https://phenix-online.org/phenix_data/afonine/qr_aimnet2_2024/). Refinement parameters are documented in README files, as well as in the Python scripts used to run the refinements. Input data for deposited models were obtained from the Protein Data Bank<sup>67</sup> and Electron Microscopy Data Bank<sup>68</sup>, either by using the Phenix tool `phenix.fetch_pdb` or from the CERES server<sup>69</sup>.

## Graphics software

Map and model images were prepared using PyMOL<sup>70</sup>. Routine inspection of maps and models was performed using Coot<sup>71</sup>. Plots were generated using Matplotlib<sup>72</sup>.

## Acknowledgements

PVA, NWM, and PDA acknowledge funding from the National Institutes of Health (grants R01GM071939, P01GM063210, and R24GM141254), as well as support from the Phenix Industrial Consortium and the US Department of Energy under Contract No. DE-AC02-05CH11231. OI acknowledges support from the US National Science Foundation (NSF CHE-2154447). AER acknowledges support from the US National Science Foundation (NSF CHE-1802831 and OAC-2311632). MB acknowledges support from the COST Action CA21101 “Confined molecular systems: from a new generation of materials to the stars’ (COSY)” supported by COST (European Cooperation in Science and Technology).

This work used Expanse at SDSC and Bridges-2 at PSC through allocation CHE200122 from the Advanced Cyberinfrastructure Coordination Ecosystem: Services & Support (ACCESS) program, which is supported by NSF grants #2138259, #2138286, #2138307, #2137603, and #2138296. This research is part of the Frontera computing project at the Texas Advanced Computing Center. Frontera is made possible by the National Science Foundation award OAC-1818253. This research, in part, was done using resources provided by the Open Science Grid, which is supported by the award 1148698 and the U.S. DOE Office of Science.

### **Author contributions**

Conceptualization: P.V.A., A.E.R., O.I., M.B.; Methodology: R.Z., H.G., K.R.; Software: P.V.A., N.W.M., R.Z., M.P.V., H.K.; Validation: M.B., K.R., H.G., P.D.A.; Formal analysis: M.B.; Data Curation: R.Z., H.G., K.R., P.V.A.; Writing (original draft): P.V.A., M.B., R.Z.; Writing (review & editing): all authors; Visualization: P.V.A., M.B., H.G., R.Z.; Supervision, P.V.A., A.E.R., O.I.; Project administration: P.V.A., A.E.R., O.I., M.B.; Funding Acquisition: P.D.A., P.V.A., A.E.R., O.I.

### **Competing Interests**

The authors declare no competing interests.

## References

1. Abramson, J. *et al.* Accurate structure prediction of biomolecular interactions with AlphaFold 3. *Nature* **630**, 493–500 (2024).
2. Baek, M. *et al.* Accurate prediction of protein structures and interactions using a three-track neural network. *Science* **373**, 871–876 (2021).
3. Krishna, R. *et al.* Generalized biomolecular modeling and design with RoseTTAFold All-Atom. *Science* **384**, eadl2528 (2024).
4. Terwilliger, T. C. *et al.* AlphaFold predictions are valuable hypotheses and accelerate but do not replace experimental structure determination. *Nat. Methods* **21**, 110–116 (2024).
5. Edich, M., Briggs, D. C., Kippes, O., Gao, Y. & Thorn, A. The impact of AlphaFold2 on experimental structure solution. *Faraday Discuss.* **240**, 184–195 (2022).
6. Urzhumtsev, A. G. & Lunin, V. Y. Introduction to crystallographic refinement of macromolecular atomic models. *Crystallogr. Rev.* **25**, 164–262 (2019).
7. Evans, P. R. An introduction to stereochemical restraints. *Acta Crystallogr. D Biol. Crystallogr.* **63**, 58–61 (2007).
8. Vagin, A. A. *et al.* REFMAC 5 dictionary: organization of prior chemical knowledge and guidelines for its use. *Acta Crystallogr. D Biol. Crystallogr.* **60**, 2184–2195 (2004).
9. Engh, R. A. & Huber, R. Accurate bond and angle parameters for X-ray protein structure refinement. *Acta Crystallogr. A* **47**, 392–400 (1991).

10. Agirre, J. *et al.* The CCP 4 suite: integrative software for macromolecular crystallography. *Acta Crystallogr. Sect. Struct. Biol.* **79**, 449–461 (2023).
11. Liebschner, D. *et al.* Macromolecular structure determination using X-rays, neutrons and electrons: recent developments in *Phenix*. *Acta Crystallogr. Sect. Struct. Biol.* **75**, 861–877 (2019).
12. Afonine, P. V. *et al.* Real-space refinement in *PHENIX* for cryo-EM and crystallography. *Acta Crystallogr. Sect. Struct. Biol.* **74**, 531–544 (2018).
13. Kovalevskiy, O., Nicholls, R. A. & Murshudov, G. N. Automated refinement of macromolecular structures at low resolution using prior information. *Acta Crystallogr. Sect. Struct. Biol.* **72**, 1149–1161 (2016).
14. DeLaBarre, B. & Brunger, A. T. Considerations for the refinement of low-resolution crystal structures. *Acta Crystallogr. D Biol. Crystallogr.* **62**, 923–932 (2006).
15. Headd, J. J. *et al.* Use of knowledge-based restraints in *phenix.refine* to improve macromolecular refinement at low resolution. *Acta Crystallogr. D Biol. Crystallogr.* **68**, 381–390 (2012).
16. Sobolev, O. V., Afonine, P. V., Adams, P. D. & Urzhumtsev, A. Programming new geometry restraints: parallelity of atomic groups. *J. Appl. Crystallogr.* **48**, 1130–1141 (2015).
17. De Vries, I. *et al.* New restraints and validation approaches for nucleic acid structures in *PDB-REDO*. *Acta Crystallogr. Sect. Struct. Biol.* **77**, 1127–1141 (2021).
18. Afonine, P. V., Sobolev, O. V., Moriarty, N. W., Terwilliger, T. C. & Adams, P. D. Overall protein structure quality assessment using hydrogen-bonding parameters. *Acta Crystallogr. Sect. Struct. Biol.* **79**, 684–693 (2023).

19. Moriarty, N. W., Liebschner, D., Tronrud, D. E. & Adams, P. D. Arginine off-kilter: guanidinium is not as planar as restraints denote. *Acta Crystallogr. Sect. Struct. Biol.* **76**, 1159–1166 (2020).
20. Richardson, J. S. *et al.* Model validation: local diagnosis, correction and when to quit. *Acta Crystallogr. Sect. Struct. Biol.* **74**, 132–142 (2018).
21. Jiang, Z., Biczysko, M. & Moriarty, N. W. Accurate geometries for “Mountain pass” regions of the Ramachandran plot using quantum chemical calculations. *Proteins Struct. Funct. Bioinforma.* **86**, 273–278 (2018).
22. Moriarty, N. W. *et al.* Improved chemistry restraints for crystallographic refinement by integrating the Amber force field into *Phenix*. *Acta Crystallogr. Sect. Struct. Biol.* **76**, 51–62 (2020).
23. Zheng, M., Reimers, J. R., Waller, M. P. & Afonine, P. V. Q | R: quantum-based refinement. *Acta Crystallogr. Sect. Struct. Biol.* **73**, 45–52 (2017).
24. Bergmann, J., Oksanen, E. & Ryde, U. Combining crystallography with quantum mechanics. *Curr. Opin. Struct. Biol.* **72**, 18–26 (2022).
25. Zheng, M. *et al.* Including crystallographic symmetry in quantum-based refinement: Q | R #2. *Acta Crystallogr. Sect. Struct. Biol.* **76**, 41–50 (2020).
26. Zheng, M. *et al.* Solving the scalability issue in quantum-based refinement: Q|R#1. *Acta Crystallogr. Sect. Struct. Biol.* **73**, 1020–1028 (2017).
27. Wang, L. *et al.* Real-space quantum-based refinement for cryo-EM: Q | R #3. *Acta Crystallogr. Sect. Struct. Biol.* **76**, 1184–1191 (2020).
28. Borbulevych, O. Y., Plumley, J. A., Martin, R. I., Merz, K. M. & Westerhoff, L. M. Accurate macromolecular crystallographic refinement: incorporation of the linear

- scaling, semiempirical quantum-mechanics program *DivCon* into the *PHENIX* refinement package. *Acta Crystallogr. D Biol. Crystallogr.* **70**, 1233–1247 (2014).
29. Ryde, U. Combined quantum and molecular mechanics calculations on metalloproteins. *Curr. Opin. Chem. Biol.* **7**, 136–142 (2003).
30. Canfield, P., Dahlbom, M. G., Hush, N. S. & Reimers, J. R. Density-functional geometry optimization of the 150 000-atom photosystem-I trimer. *J. Chem. Phys.* **124**, 024301 (2006).
31. Kulik, H. J., Luehr, N., Ufimtsev, I. S. & Martinez, T. J. Ab Initio Quantum Chemistry for Protein Structures. *J. Phys. Chem. B* **116**, 12501–12509 (2012).
32. Zheng, M. & Waller, M. P. Adaptive quantum mechanics/molecular mechanics methods. *WIREs Comput. Mol. Sci.* **6**, 369–385 (2016).
33. Anstine, D., Zubatyuk, R. & Isayev, O. AIMNet2: A Neural Network Potential to Meet your Neutral, Charged, Organic, and Elemental-Organic Needs. Preprint at <https://doi.org/10.26434/chemrxiv-2023-296ch-v2> (2024).
34. Smith, J. S., Isayev, O. & Roitberg, A. E. ANI-1: an extensible neural network potential with DFT accuracy at force field computational cost. *Chem. Sci.* **8**, 3192–3203 (2017).
35. Smith, J. S., Nebgen, B., Lubbers, N., Isayev, O. & Roitberg, A. E. Less is more: Sampling chemical space with active learning. *J. Chem. Phys.* **148**, 241733 (2018).
36. Devereux, C. *et al.* Extending the Applicability of the ANI Deep Learning Molecular Potential to Sulfur and Halogens. *J. Chem. Theory Comput.* **16**, 4192–4202 (2020).
37. Zubatyuk, R., Smith, J. S., Nebgen, B. T., Tretiak, S. & Isayev, O. Teaching a neural network to attach and detach electrons from molecules. *Nat. Commun.* **12**, 4870

- (2021).
38. Yan, Z., Wei, D., Li, X. & Chung, L. W. Accelerating reliable multiscale quantum refinement of protein–drug systems enabled by machine learning. *Nat. Commun.* **15**, 4181 (2024).
  39. Brünger, A. T., Karplus, M. & Petsko, G. A. Crystallographic refinement by simulated annealing: application to crambin. *Acta Crystallogr. A* **45**, 50–61 (1989).
  40. Wang, Y. *et al.* Optimal clustering for quantum refinement of biomolecular structures: QR#4. *Theor. Chem. Acc.* **142**, 100 (2023).
  41. Moriarty, N. W., Tronrud, D. E., Adams, P. D. & Karplus, P. A. Conformation-dependent backbone geometry restraints set a new standard for protein crystallographic refinement. *FEBS J.* **281**, 4061–4071 (2014).
  42. Engh, R. A. & Huber, R. Structure quality and target parameters. in 474–484 (2012). doi:10.1107/97809553602060000857.
  43. Afonine, P. V. *et al.* New tools for the analysis and validation of cryo-EM maps and atomic models. *Acta Crystallogr. Sect. Struct. Biol.* **74**, 814–840 (2018).
  44. Booth, A. D. LXXIV. An expression for following the process of refinement in X-ray structure analysis using fourier series. *Lond. Edinb. Dublin Philos. Mag. J. Sci.* **36**, 609–615 (1945).
  45. Brünger, A. T. Free R value: a novel statistical quantity for assessing the accuracy of crystal structures. *Nature* **355**, 472–475 (1992).
  46. Williams, C. J. *et al.* MolProbity: More and better reference data for improved all-atom structure validation. *Protein Sci.* **27**, 293–315 (2018).
  47. Lovell, S. C. *et al.* Structure validation by C $\alpha$  geometry:  $\phi$ ,  $\psi$  and C $\beta$  deviation.

- Proteins Struct. Funct. Bioinforma.* **50**, 437–450 (2003).
48. Hintze, B. J., Lewis, S. M., Richardson, J. S. & Richardson, D. C. Molprobity's ultimate rotamer-library distributions for model validation: MolProbity's Ultimate Rotamer-Library. *Proteins Struct. Funct. Bioinforma.* **84**, 1177–1189 (2016).
49. Lovell, S. C., Word, J. M., Richardson, J. S. & Richardson, D. C. The penultimate rotamer library. *Proteins Struct. Funct. Genet.* **40**, 389–408 (2000).
50. Emsley, P., Lohkamp, B., Scott, W. G. & Cowtan, K. Features and development of *Coot*. *Acta Crystallogr. D Biol. Crystallogr.* **66**, 486–501 (2010).
51. Chen, V. B. *et al.* *MolProbity*: all-atom structure validation for macromolecular crystallography. *Acta Crystallogr. D Biol. Crystallogr.* **66**, 12–21 (2010).
52. Sobolev, O. V. *et al.* A Global Ramachandran Score Identifies Protein Structures with Unlikely Stereochemistry. *Structure* **28**, 1249-1258.e2 (2020).
53. Tickle, I. J., Laskowski, R. A. & Moss, D. S.  $R_{\text{free}}$  and the  $R_{\text{free}}$  Ratio. I. Derivation of Expected Values of Cross-Validation Residuals Used in Macromolecular Least-Squares Refinement. *Acta Crystallogr. D Biol. Crystallogr.* **54**, 547–557 (1998).
54. Tickle, I. J., Laskowski, R. A. & Moss, D. S.  $R_{\text{free}}$  and the  $R_{\text{free}}$  ratio. II. Calculation of the expected values and variances of cross-validation statistics in macromolecular least-squares refinement. *Acta Crystallogr. D Biol. Crystallogr.* **56**, 442–450 (2000).
55. Barad, B. A. *et al.* EMRinger: side chain-directed model and map validation for 3D cryo-electron microscopy. *Nat. Methods* **12**, 943–946 (2015).
56. Grosse-Kunstleve, R. W., Sauter, N. K., Moriarty, N. W. & Adams, P. D. The *Computational Crystallography Toolbox*: crystallographic algorithms in a reusable

- software framework. *J. Appl. Crystallogr.* **35**, 126–136 (2002).
57. Hawkins, P. C. D., Skillman, A. G., Warren, G. L., Ellingson, B. A. & Stahl, M. T. Conformer Generation with OMEGA: Algorithm and Validation Using High Quality Structures from the Protein Databank and Cambridge Structural Database. *J. Chem. Inf. Model.* **50**, 572–584 (2010).
58. Spicher, S. & Grimme, S. Robust Atomistic Modeling of Materials, Organometallic, and Biochemical Systems. *Angew. Chem. Int. Ed.* **59**, 15665–15673 (2020).
59. Mardirossian, N. & Head-Gordon, M. Mapping the genome of meta-generalized gradient approximation density functionals: The search for B97M-V. *J. Chem. Phys.* **142**, 074111 (2015).
60. Caldeweyher, E. *et al.* A generally applicable atomic-charge dependent London dispersion correction. *J. Chem. Phys.* **150**, 154122 (2019).
61. Weigend, F. & Ahlrichs, R. Balanced basis sets of split valence, triple zeta valence and quadruple zeta valence quality for H to Rn: Design and assessment of accuracy. *Phys. Chem. Chem. Phys.* **7**, 3297 (2005).
62. Weigend, F. Accurate Coulomb-fitting basis sets for H to Rn. *Phys. Chem. Chem. Phys.* **8**, 1057 (2006).
63. Neese, F., Wennmohs, F., Becker, U. & Riplinger, C. The ORCA quantum chemistry program package. *J. Chem. Phys.* **152**, 224108 (2020).
64. Barone, V. & Cossi, M. Quantum Calculation of Molecular Energies and Energy Gradients in Solution by a Conductor Solvent Model. *J. Phys. Chem. A* **102**, 1995–2001 (1998).
65. Word, J. M., Lovell, S. C., Richardson, J. S. & Richardson, D. C. Asparagine and

glutamine: using hydrogen atom contacts in the choice of side-chain amide

orientation 1 1 Edited by J. Thornton. *J. Mol. Biol.* **285**, 1735–1747 (1999).

66. Afonine, P. V. *et al.* Towards automated crystallographic structure refinement with *phenix.refine*. *Acta Crystallogr. D Biol. Crystallogr.* **68**, 352–367 (2012).
67. Berman, H. M. The Protein Data Bank. *Nucleic Acids Res.* **28**, 235–242 (2000).
68. The wwPDB Consortium *et al.* EMDB—the Electron Microscopy Data Bank. *Nucleic Acids Res.* **52**, D456–D465 (2024).
69. Liebschner, D. *et al.* *CERES*: a cryo-EM re-refinement system for continuous improvement of deposited models. *Acta Crystallogr. Sect. Struct. Biol.* **77**, 48–61 (2021).
70. Schrödinger, LLC. The PyMOL Molecular Graphics System, Version 1.8. (2015).
71. Emsley, P. & Cowtan, K. *Coot*: model-building tools for molecular graphics. *Acta Crystallogr. D Biol. Crystallogr.* **60**, 2126–2132 (2004).
72. Hunter, J. D. Matplotlib: A 2D Graphics Environment. *Comput. Sci. Eng.* **9**, 90–95 (2007).

